Noname manuscript No.
(will be inserted by the editor)

Active Contours with Free Endpoints

Hayden Schaeffer · Luminita Vese

Received: date / Accepted: date

1 Introduction

Image segmentation is one of the most important yet challenging problems in imaging science. The goal of segmentation is to locate important edges and boundaries in an image. The difficulty resides in the notion of the edge or boundary set, and thus the definition of segmentation itself. One way to define segmentation is as the process of partitioning up an image into different features or objects. In this way, the edge set must be made up of curves with no endpoints (loops) or that terminate at the boundaries of the image domain. An alternative definition, one that is employed by many mathematical segmentation techniques, is the location of boundaries between important features and objects. The latter is more general, since the boundary set may contain curves with free endpoints which do not partition the domain in the classical sense. In this paper, we propose an extension to the classical level set based segmentation techniques which allow for the more general class of boundaries, including curves with free endpoints. We will do so by extending the active contours models [5,34], using a different formulation of the edge set which can capture a large class of edges.

The Mumford and Shah model (MS) is defined as follows: find a piecewise smooth approximation, u, of a given image f, which may have jumps along a set Γ by minimizing the following:

$$\inf_{u,\Gamma} E_{MS}(u,\Gamma) = \mu \int_{\Omega\setminus\Gamma} |\nabla u|^2 dx + \gamma \int_{\Omega} |u-f|^2 dx + \lambda \mathcal{H}^1(\Gamma) \tag{1}$$

The first term requires u to be smooth outside of the jump set Γ, the second term ensures that u remains close to f in the L^2 sense, and the last term is the Hausdorff measure ("length") of the jump set which regularizes the edge set. Theoretical results on the existence and regularity of minimizers can be found in the works of Morel and Solimini [21,22], Dal Maso, Morel, Solimini [9], and De Giorgi, Carriero and Leaci [12]. Specifically, the edge set is made up of $C^{1,1}$ segments whose endpoints either terminate perpendicularly to the boundary of the domain, terminate at a triple junction where three segments connect, or terminate at a free endpoint where the segment does not connect to any other edges.

Based on Γ-convergence [1], Ambrosio and Tortorelli proposed an elliptic approximation to the Mumford and Shah model. The set Γ is replaced by a function $v \in [0,1]$, which is 1 away from an edge and 0 on an edge, thus acting as an indicator function. The approximated functional is:

$$\inf_{u,v} E_{AT}(u,v) = \mu \int_{\Omega} (v^2+\eta_\epsilon)|\nabla u|^2 dx + \gamma \int_{\Omega} |u-f|^2 dx + \lambda \int_{\Omega} \left(\frac{\epsilon}{2}|\nabla v|^2 dx + \frac{1}{2\epsilon}|v-1|^2 \right) dx \tag{2}$$

where $\epsilon > 0$ is a small parameter and $\eta_\epsilon = o(\epsilon)$. The last integral replaces the length term and enforces that the function v is smooth and close to 1 except for a small region around an edge. It can be shown that as $\epsilon \to 0$ the functional above Γ-converges to the weak formulation of the Mumford and Shah functional. One advantage of this formulation over the level set based methods is that the edge set can contain all types

University of California, Los Angeles
Department of Mathematics
Los Angeles, CA 90095, USA
E-mail:

of curves theoretically possible as minimizers of the Mumford and Shah model. On the other hand, since the indicator function v does not sharply define edges, the reconstructed image may not have sharp jumps. The width of the edge is determined by the parameter ϵ, which may also cause thickening of the edge set. This was extended in [30] to include a texture regularizer.

In this work, our proposed model is formulated using the Level Set method, proposed by Osher and Sethian [27]. The level set method provides an implicit representation for curves by defining them as the zero level set of a Lipschitz continuous function $\phi : \Omega \to \mathbb{R}$. Using the level set framework allows the curve to undergo changes in topology and allows for the formation of cusps and corners. The level set method does restrict the class of possible edge sets to curves made up of segments without endpoints or that terminate at the boundary of the domain.

In [5],the authors proposed a region based segmentation and restoration method formulated within the level set framework. The reconstructed image u is defined as a piecewise constant function, equal to c_1 inside the region enclosed by the curve and c_2 outside the region enclosed by the curve. The energy minimization is as follows:

$$\inf_{c_1,c_2,\Gamma} E_{CV}(c_1,c_2,\Gamma) = \gamma_1 \int_{inside(\Gamma)} |f-c_1|^2 dx + \gamma_2 \int_{outside(\Gamma)} |f-c_2|^2 dx + \lambda \text{Length}(\Gamma) \tag{3}$$

The first two terms enforce that the given image f must remain close to the constants c_1 and c_2 in each region of their respective regions. When minimized, the last term regularizes the edge set by making it as small as possible while still separating the two regions. Equation (3) is a special case of the Mumford and Shah functional [23], in which the reconstructed image is restricted to the class of piecewise constant solutions.

In [34], the authors proposed an extension of the original active contours model without edges, providing a practical implementation of the full Mumford and Shah model. Two level set functions are used to define four regions and the reconstructed function u is defined piecewise by four auxiliary functions u_j, $1 \le j \le 4$, which are smooth in each of their respective regions. The model is as follows:

$$\begin{aligned}\inf_{u_j,\Gamma} E_{VC}(u_j,\Gamma) = \mu \left\{ \int_{\Omega_1} |\nabla u_1|^2 dx + \mu \int_{\Omega_2} |\nabla u_2|^2 dx + \mu \int_{\Omega_3} |\nabla u_3|^2 dx + \mu \int_{\Omega_4} |\nabla u_4|^2 dx \right\} \\ +\gamma \left\{ \int_{\Omega_1} |u_1 - f|^2 dx + \mu \int_{\Omega_2} |u_2 - f|^2 dx + \mu \int_{\Omega_3} |u_3 - f|^2 dx + \mu \int_{\Omega_4} |u_4 - f|^2 dx \right\} + \lambda \text{Length}(\Gamma)\end{aligned} \tag{4}$$

and the regions $\Omega_1, ..., \Omega_4$ are represented using two open sets. The minimizing function u is smooth outside of the set Γ, where it may have jumps. The minimizing edge set Γ is comprised of curves that terminate perpendicularly to the boundary of the domain and curves without endpoints, but cannot have curves with free endpoints. See also [33] for parellel related work, [3] for an alternative model based on geodesics, and [4] for an extension to vector valued images.

An alternative level set formulation can be found in [6], where the authors proposed a multilayer extension to the piecewise constant active contours model. Their model uses multiple level lines of ϕ in order to segment many embedded objects. The resulting reconstructed image is piecewise constant and the resulting edge set is comprised of curves that terminate perpendicularly to the boundary of the domain and curves without endpoints which may be enclosed in each other.

The level set based segmentation methods thus far are unable to located edges with free endpoints. In this paper, we propose an extension to the level set techniques for segmentation by defining a more general edge set. Using the method from the work of Smereka [31] to represent curves with endpoints, we propose a level set based segmentation method which can capture free curves, in addition to all previously possible curves. Related work on free curves can be found in [7, 14–18, 20].

The paper is organized as follows. Chapter 2 provides a description of the model with our particular curve and function representation. Also, a brief description of Sobolev gradients and its application to our equations is provided. In Chapter 3, some analytical remarks on the model and its relation to other level models are discussed. The numerical techniques and algorithm are presented in Chapter 4, with experimental results on both synthetic and real images in Chapter 5.

2 Description of the Proposed Model

Before discussing the model, the level set method with addition of free curves will be reviewed. After that, the energy will be presented with the associated equations of motion. Lastly, we will review the theory of Sobolev gradients and its application to our evolution equations.

2.1 Representation of Curves with Free Endpoints and Domain Partitioning

Osher and Sethian proposed the level set method as an implicit representation of curves [27]. In the classical level set formulation, a curve Γ is represented as the zero level set of a Lipschitz continuous function, $\phi : \Omega \to \mathbb{R}$. The assumption is that Γ is the boundary of an open set, and thus Γ is comprised of curves without endpoints and curves which terminate at the boundary of the domain. The interior region is defined as the set of points where $\phi > 0$ and the exterior region is defined as the set of points where $\phi < 0$. The standard example of a level set function is the signed distance function to the curve.

Using the Heaviside function, defined as $H(s) = 1$, if $s \geq 0$, and $H(s) = 0$, if $s < 0$, in conjunction with the level set function, one can reformulate geometric quantities into easier-to-handle equations. Instead of looking at quantities along the curve, ϕ allows the calculations to be extended to the entire domain, making calculations more practical. For example, the length of the curve and the area enclosed by the curve can be written as:

$$L(\Gamma) = \int |\nabla H(\phi)|, \qquad A(\Gamma) = \int H(\phi)dx$$

The derivative of the Heaviside function is taken in the sense of measures. The problem can be regularized by taken a differentiable approximation, H_ϵ, which limits to the Heaviside function as $\epsilon \to 0$. This provides an approximation to the Dirac delta function, $\delta_\epsilon = H'_\epsilon$, and the quantities above can be approximated:

$$L_\epsilon(\Gamma) = \int \delta_\epsilon(\phi)|\nabla\phi|dx, \qquad A_\epsilon(\Gamma) = \int H_\epsilon(\phi)dx$$

These equations can then be minimized by introducing an artificial time and descending using (the negative) of the Euler-Lagrange equations respectively:

$$\frac{\partial\phi}{\partial t} = \delta_\epsilon(\phi)\mathrm{div}\left(\frac{\nabla\phi}{|\nabla\phi|}\right) \qquad \frac{\partial\phi}{\partial t} = -\delta_\epsilon(\phi)$$

Since the delta function's approximation is assumed to be strictly positive, the equations can be rescaled to the following equations, which have the same steady state solutions as the equations above:

$$\frac{\partial\phi}{\partial t} = |\nabla\phi|\mathrm{div}\left(\frac{\nabla\phi}{|\nabla\phi|}\right), \qquad \frac{\partial\phi}{\partial t} = -|\nabla\phi|$$

The length minimizing equation is the mean curvature flow, while the area minimizing equation is a Hamilton-Jacobi equation. Each of the two equations above play an important role in level set based segmentation models. For example, let us consider the Chan-Vese model:

$$E_{CV}(c_1, c_2, \phi) = \lambda \int \delta(\phi)|\nabla\phi|dx + \int \Big((c_1 - f)^2 H(\phi) + (c_2 - f)^2 (1 - H(\phi))\Big)\, dx$$

In terms of ϕ, the length term acts as the regularizer while the area terms are connected to the regional fidelity terms. Each region is clearly defined by the level set function, where the sign determines the regions. Using the same formulation, the two phase piecewise smooth Vese-Chan model is:

$$\begin{aligned} E_{VC}(u_1, u_2, \phi) = \lambda \int \delta(\phi)|\nabla\phi|dx + \int \Big((u_1 - f)^2 H(\phi) + (u_2 - f)^2 (1 - H(\phi))\Big)\, dx \\ +\mu \int \Big(|\nabla u_1|^2 H(\phi) + |\nabla u_1|^2 (1 - H(\phi))\Big)\, dx. \end{aligned}$$

Again, the level set function partitions the domain into two regions. This partitioning allows the function u, which is an approximation of f, to have clearly defined jumps. In this paper, we wish to further extend the level set based segmentation methods to allow for jumps on curves with free endpoints. This is done by introducing a second level set function ψ, which acts as an indicator function partitioning up the zero level

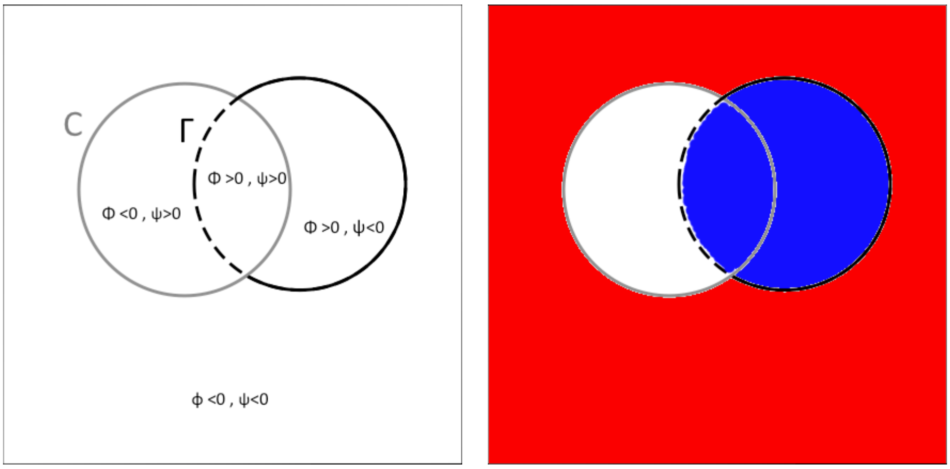

(a) Level Set Representation of the Curve Γ, the dotted line above

(b) Color Coded Partition of Space

Fig. 1 Level Set Representation of the curve Γ, with free endpoints

set of ϕ into two segments (see Figure 1 a), based on the work of Smereka [31]. The curve Γ is defined as $\{(x,y) \in \Omega \mid \phi(x,y) = 0 \text{ and } \psi(x,y) > 0\}$, which now allows the curve to have loops, segments terminating at the boundary of the domain, and segments with free endpoints. Revisiting the length functional from before, the new formulation is as follows:

$$L(\Gamma) = \int |\nabla H(\phi)| H(\psi), \qquad L_\epsilon(\Gamma) = \int \delta_\epsilon(\phi) H_\epsilon(\psi) |\nabla \phi| dx,$$

The length can be minimized by descending using the first variation:

$$\begin{aligned}\frac{\partial \phi}{\partial t} &= \delta(\phi) \text{div} \left(H(\psi) \frac{\nabla \phi}{|\nabla \phi|} \right) \\ \frac{\partial \psi}{\partial t} &= -\delta(\psi)\delta(\phi)|\nabla \phi|,\end{aligned}$$

assuming the Heaviside and Dirac delta functions are replaced by their smooth counterparts. The standard rescaled versions become:

$$\begin{aligned}\frac{\partial \phi}{\partial t} &= |\nabla \phi| \text{div} \left(H(\psi) \frac{\nabla \phi}{|\nabla \phi|} \right) \\ \frac{\partial \psi}{\partial t} &= -\delta(\phi)|\nabla \phi||\nabla \psi|.\end{aligned}$$

The equation for ϕ defines a mean curvature flow, while the equation ψ defines an area minimizing Hamilton-Jacobi equation.

Although similar in structure, there is a key difference between the classical and the proposed formulations – in the proposed case, the domain does not have a natural partition, since there is no clear concept of the interior and exterior of Γ. A proper partition for the domain should enforce that the reconstructed function only has jumps along the curve, so one choice (and the choice we use in this paper) is to divide the domain in three regions: region 0: $\phi < 0$ and $\psi < 0$ (red in Figure 1 b), region 1: $\phi > 0$ (blue in Figure 1 b), and region 2: $\phi < 0$ and $\psi > 0$ (white in Figure 1 b). In this way, the important boundary is the one separating the white and blue region. As in the classical formulation, two auxiliary functions u_1 and u_2 are chosen so that each function is smooth in their respective regions, but unlike the other methods, they must be smooth over the zero level curves outside of $\phi = 0$ and $\psi > 0$. If we define the reconstructed image as a linear combination of the two auxiliary functions, then choosing the partition in this manner ensures that the only discontinuities in u lie on Γ. If we denote the regions using the following characteristic functions: $\chi_1 = H(\phi)$, $\chi_2 = H(\psi)(1 - H(\phi))$, and $\chi_0 = (1 - H(\psi))(1 - H(\phi))$, then u_1 exists in region 0 and region 1 and u_2 exists in region 0 and region 2. The reconstructed function becomes:

$$u = u_1\chi_1 + u_2\chi_2 + \left(\frac{u_1+u_2}{2}\right)\chi_0 \tag{5}$$

where the two auxiliary functions are averaged in region 0, although any non-trivial linear combination is sufficient. Using the partition and function above, we can formulate the level set based MS energy for a general curve.

2.2 The Energy

Recall that the MS energy in terms of the reconstructed image u and jump set Γ, with given (possibly corrupt) image f is:

$$E_{MS}(u,\Gamma) = \mu\int_{\Omega\setminus\Gamma} |\nabla u|^2 dx + \lambda\mathcal{H}^1(\Gamma) + \int_\Omega |u-f|^2 dx.$$

Using equation (5) and our definition of Γ the energy becomes:

$$\begin{aligned} E(u_1,u_2,\phi,\psi) = \mu\int_\Omega \left(|\nabla u_1|^2(\chi_1 + \frac{\chi_0}{4}) + |\nabla u_2|^2(\chi_2 + \frac{\chi_0}{4}) + \frac{1}{2}\nabla u_1\cdot\nabla u_2\chi_0\right)dx + \lambda\int_\Omega \chi_3\ |\nabla\chi_1| \\ + \int_\Omega \left(|u_1-f|^2\chi_1 + |u_2-f|^2\chi_2 + \left|\frac{u_1+u_2}{2} - f\right|^2\chi_0\right)dx \end{aligned}$$

where $\chi_3 = H(\psi)$ and all measure zero terms are ignored. The first three terms are the regional regularities of the reconstructed function, the fourth term is the length regularity for the curve, and the last three terms are the regional fidelity terms. The average of the auxiliary function is necessary to ensure that both functions are smooth over the non-essential zero level sets. For the sake of argument, let us assume the reconstructed function u is exactly u_o (the original image), and, instead of an average, we took the sum of the auxiliary: $u = u_1\chi_1 + u_2\chi_2 + (u_1+u_2)\chi_0$. Then we have the following: in region 1 $u_1 = u_o$, in region 2 $u_2 = u_o$, and in region 0 $u_1 + u_2 = u_o$. For this to be possible, one of the functions must take values that are at most half of u_o, so that function's values would sharply decrease over the boundary between region 1 or 2 and region 0. By taking the average, neither function may have jumps over the non-essential zero level sets.

Next, assuming that the Heaviside functions are regularized, the Euler-Lagrange equations are as follows:

$$\begin{cases} \frac{\partial u_j}{\partial t} &= \mu\ \mathrm{div}\left(2\chi_j\nabla u_j + \frac{\chi_0}{2}\nabla(u_1+u_2)\right) - 2(u_j-f)\chi_j - \left(\frac{u_1+u_2}{2} - f\right)\chi_0 \\ \frac{\partial\phi}{\partial t} &= \delta(\phi)\Big\{\lambda\mathrm{div}\left(\chi_3\frac{\nabla\phi}{|\nabla\phi|}\right) - |u_1-f|^2 + \chi_3|u_2-f|^2 + (1-\chi_3)\left|\frac{u_1+u_2}{2} - f\right|^2 \\ &\qquad -\mu|\nabla u_1|^2\left(\frac{3}{4} + \frac{\chi_3}{4}\right) + \mu|\nabla u_2|^2\left(\frac{1}{4} + \frac{3\chi_3}{4}\right) + \frac{1}{2}\mu\nabla u_1\cdot\nabla u_2(1-\chi_3)\Big\} \\ \frac{d\psi}{dt} &= -\delta(\psi)\left\{\lambda|\nabla\chi_1| + (1-\chi_1)\Big(|u_2-f|^2 - \left|\frac{u_1+u_2}{2} - f\right|^2 - \frac{\mu}{4}|\nabla u_1|^2 + \frac{3\mu}{4}|\nabla u_2|^2 - \frac{\mu}{2}\nabla u_1\cdot\nabla u_2\Big)\right\} \end{cases}$$

with the following boundary conditions:

$$\begin{cases} \chi_j\frac{\partial u_j}{\partial n} + \frac{1}{4}\chi_0\frac{\partial}{\partial n}(u_1+u_2) &= 0 \\ \frac{\chi_3}{|\nabla\phi|}\frac{\partial\phi}{\partial n} &= 0 \end{cases}$$

and the initial conditions: $u_j(0,x) = u_j^0(x)$, $\phi(0,x) = \phi^0(x)$, and $\psi(0,x) = \psi^0(x)$. For simplicity, the boundary condition can be reduced to the standard Neumann boundary condition, which we will show in Section 4. The system of PDEs include diffusion equations for u_1 and u_2, mean curvature flow for ϕ and the area minimizing ODE for ψ. As before, the level set functions' PDE can be rescaled by the magnitudes of their gradients.

Remark 1 Although not always necessary, in practice, extra regularization on the level set functions may ensure a smoother evolution. For example, the following regularized PDEs give a smoother flow for the system above:

$$\begin{cases} \frac{\partial \phi}{\partial t} &= \delta(\phi)\Big\{\lambda \mathrm{div}\left((\chi_3+\epsilon_1)\frac{\nabla\phi}{|\nabla\phi|}\right) - |u_1-f|^2 + \chi_3|u_2-f|^2 + (1-\chi_3)\left|\frac{u_1+u_2}{2}-f\right|^2 \\ & \qquad -\mu|\nabla u_1|^2\left(\frac{3}{4}+\frac{\chi_3}{4}\right) + \mu|\nabla u_2|^2\left(\frac{1}{4}+\frac{3\chi_3}{4}\right) + \frac{1}{2}\mu\nabla u_1\cdot\nabla u_2(1-\chi_3)\Big\} \\ \frac{\partial \psi}{\partial t} &= \delta(\psi)\left\{\epsilon_2 \Delta_\infty\psi - \lambda|\nabla\chi_1| + (1-\chi_1)\Big(|u_2-f|^2 - \left|\frac{u_1+u_2}{2}-f\right|^2 - \frac{\mu}{4}|\nabla u_1|^2 + \frac{3\mu}{4}|\nabla u_2|^2 - \frac{\mu}{2}\nabla u_1\cdot\nabla u_2\Big)\right\} \end{cases}$$

where ϵ_1 and ϵ_2 are (small) parameters and $\Delta_\infty\psi = \left\langle \frac{\nabla\psi}{|\nabla\psi|}, D^2\psi\frac{\nabla\psi}{|\nabla\psi|}\right\rangle$ is the renormalized infinity Laplacian. In terms of energy minimization, this is equivalent to adding a length regularizer on the zero level curve of ϕ and an (rescaled) infinity norm regularizer for $|\nabla\psi|$. For more details of related to the theory of the infinity Laplacian, see [8, 11, 19] and for discretizations see [26].

2.3 Sobolev Gradient

In order to minimize the proposed energy, a gradient descent method is used. The first variation (or Euler-Lagrange equation) is imbedded in a dynamic scheme as follows: given an energy $E(\phi)$ with Euler-Lagrange equations that are denoted as $\nabla_{L^2}E(\phi)$, the gradient descent is $\frac{\partial\phi}{\partial t} = -\nabla_{L^2}E(\phi)$. For a general energy, this PDE may not be well-posed and could lead to many issues. To better pose the equation, the Sobolev Gradient, denoted as $\nabla_{H^1}E(\phi)$ can be used. Here we provide a short derivation, following Neuberger [24] and Renka [28]. Assume that the energy can be written with a potential V as $E(\phi) = \int_\Omega V(D\phi)dx$ and it is to be minimized over $H^1(\Omega)$, where $D: H^1(\Omega) \to H^1(\Omega)\times L^2(\Omega)$ is the operator $D\phi = (\phi, \nabla\phi)^T$.

For all $\phi \in H^1(\Omega)$ and for any $h \in H^1_0(\Omega)$, the directional derivative is:

$$(E'(\phi), h) = \int_\Omega V'(D\phi)Dh dx = \langle \nabla V(D\phi), Dh\rangle_{L^2} = \langle D^*\nabla V(D\phi), h\rangle_{L^2}$$

where D^* is the adjoint of D. Assuming that all the terms above are in $L^2(\Omega)$, the L^2 gradient is defined as $\nabla_{L^2}E(\phi) := D^*\nabla V(D\phi)$ (which is the standard Euler-Lagrange equation). On the other hand, we can equate the L^2 inner product with the H^1 inner product in terms of the Sobolev gradient:

$$(E'(\phi), h) = \langle \nabla_{L^2}E(\phi), h\rangle_{L^2} = \langle \nabla_{H^1}E(\phi), h\rangle_{H^1}.$$

Using the operator D:

$$\langle \nabla_{H^1}E(\phi), h\rangle_{H^1} = \langle D(\nabla_{H^1}E(\phi)), Dh\rangle_{L^2} = \langle D^*D(\nabla_{H^1}E(\phi)), h\rangle_{L^2}$$

which yields: $\nabla_{H^1}E(\phi) = (D^*D)^{-1}(\nabla_{L^2}E(\phi)) = (I-\Delta)^{-1}(\nabla_{L^2}E(\phi))$ (the Sobolev gradient). This is interpreted as a gradient descent with respect to a more appropriate inner product space. This can also be seen as a preconditioned descent, with the smoothing operator $(I-\Delta)^{-1}$.

This smoothing allows the Euler-Lagrange equations to reside in a large function class. Recall that the dual of $H^1(\Omega)$, denoted $H^{-1}(\Omega) := (H^1(\Omega))^*$ (assuming Neumann boundary conditions), is larger than L^2, since it contains weaker functions. The operator $(I-\Delta)^{-1}$ can be considered as a map from $H^{-1}(\Omega) \to H^1(\Omega)$ such that for $G \in H^{-1}(\Omega)$, there exists (by Lax-Milgram) a unique $v \in H^1(\Omega)$ which solves the weak problem:

$$v - \Delta v = G \tag{6}$$

with Neumann boundary conditions. Thus for all $\nabla_{L^2}E(\phi) \in H^{-1}(\Omega)$, we can find a $\nabla_{H^1}E(\phi) \in H^1(\Omega)$. Now lets examine this in terms of the evolution equations, which define an iterative process. In the semi-discrete case, we construct the sequence ϕ^n by $\phi^{n+1} = \phi^n - \Delta t\nabla_{L^2}E(\phi^n)$, with $\phi^0 \in H^1(\Omega)$ and $\Delta t > 0$, such that $E(\phi^{n+1}) < E(\phi^n)$. In order to have $\phi^{n+1} \in H^1(\Omega)$, this would require that $\nabla_{L^2}E(\phi^n) \in H^1(\Omega) \subset L^2(\Omega)$, in other words, we would assume too strong regularity for the solution ϕ, which may not hold. This is one of the reasons for the small time-steps necessary for stability when using the L^2 gradient descent. In terms of the energy minimization, the following theorem provides further benefits of the Sobolev gradient.

Theorem 1 *For all $t > 0$, let ϕ and ϕ_s be the solution of the L^2 gradient descent ($\frac{\partial \phi}{\partial t} = -\nabla_{L^2} E(\phi)$) and Sobolev gradient descent equation ($\frac{\partial \phi_s}{\partial t} = -\nabla_{H^1} E(\phi_s)$), respectively; then:*

$$\frac{dE(\phi)}{dt} = -||\nabla_{L^2} E(\phi)||^2_{L^2}$$
$$\frac{dE(\phi_s)}{dt} = -||\nabla_{H^1} E(\phi_s)||^2_{H^1}$$

Proof Assume that $E(\phi) = \int_\Omega V(D\phi)$ then we can formally take the time derivative as follows:

$$\begin{aligned}
\frac{dE(\phi)}{dt} &= \int_\Omega \nabla_{L^2} E(\phi) \frac{\partial \phi}{\partial t} dx \\
&= -\int_\Omega |\nabla_{L^2} E(\phi)|^2 \, dx \\
&= -||\nabla_{L^2} E(\phi)||^2_{L^2}
\end{aligned}$$

The equations above hold if $\nabla_{L^2} E(\phi) \in L^2(\Omega)$. Next, taking the Sobolev gradient descent:

$$\begin{aligned}
\frac{dE(\phi_s)}{dt} &= \int_\Omega \nabla_{L^2} E(\phi_s) \frac{\partial \phi_s}{\partial t} dx \\
&= -\int_\Omega \left((I - \Delta) \frac{\partial \phi_s}{\partial t} \right) \frac{\partial \phi_s}{\partial t} dx \\
&= -\int_\Omega \left(\left| \frac{\partial \phi_s}{\partial t} \right|^2 + \left| \nabla \frac{\partial \phi_s}{\partial t} \right|^2 \right) dx \\
&= -\left|\left| \frac{\partial \phi_s}{\partial t} \right|\right|^2_{H^1} \\
&= -||\nabla_{H^1} E(\phi_s)||^2_{H^1}
\end{aligned}$$

assuming that all terms satisfy Neumann boundary conditions. The equation above holds if $\nabla_{L^2} E(\phi_s) \in H^{-1}(\Omega)$.

In terms of our model, applying this to our system of equations yields:

$$\begin{cases}
\frac{\partial u_j}{\partial t} &= (I - \Delta)^{-1} \left\{ \mu \text{ div} \left(2\chi_j \nabla u_j + \frac{\chi_0}{2} \nabla (u_1 + u_2) \right) - 2(u_j - f)\chi_j - \left(\frac{u_1 + u_2}{2} - f \right) \chi_0 \right\} \\
\frac{\partial \phi}{\partial t} &= (I - \Delta)^{-1} \Big\{ \delta(\phi) \Big(\lambda \text{div} \left(\chi_3 \frac{\nabla \phi}{|\nabla \phi|} \right) - |u_1 - f|^2 + \chi_3 |u_2 - f|^2 + (1 - \chi_3) \left| \frac{u_1 + u_2}{2} - f \right|^2 \\
& \qquad -\mu |\nabla u_1|^2 \left(\frac{3}{4} + \frac{\chi_3}{4} \right) + \mu |\nabla u_2|^2 \left(\frac{1}{4} + \frac{3\chi_3}{4} \right) + \frac{1}{2} \mu \nabla u_1 \cdot \nabla u_2 (1 - \chi_3) \Big) \Big\} \\
\frac{\partial \psi}{\partial t} &= -(I - \Delta)^{-1} \left\{ \delta(\psi) \left(\lambda |\nabla \chi_1| + (1 - \chi_1) \Big(|u_2 - f|^2 - \left| \frac{u_1 + u_2}{2} - f \right|^2 - \frac{\mu}{4} |\nabla u_1|^2 + \frac{3\mu}{4} |\nabla u_2|^2 - \frac{\mu}{2} \nabla u_1 \cdot \nabla u_2 \Big) \right) \right\}
\end{cases}$$

The versions above are used in practice. In terms of the equation in u_j, the Sobolev gradient's application is clear. For the other two equations, this may not be the case. In the case of ϕ, since the Dirac delta function and the characteristic functions are smooth and strictly positive and (for many applications) $|\nabla \phi| = 1$ a.e., the equation resembles a typical anisotropic diffusion equation, which exists in H^{-1}. Another interpretation is that, in terms of the level set functions, the delta function acts to concentrate the motion around the zero level sets, whose width is dependent on the smoothness of the approximations. The operator, $(I - \Delta)^{-1}$ in turn, continues to smooth the main area of influence of the delta function. With respect to equation (6), it is easy to show that the equation can be re-written as an optimization problem:

$$\inf_v E(v) = \int |\nabla v|^2 dx + \int |v - G|^2 dx$$

For a simple example, take G to be a smooth and strictly positive version of the Dirac delta function. Then it can be shown that $v \geq 0$, $\int v dx = \int G dx$, and $||v||_\infty \leq ||G||_\infty$. In this way, v is a smoother and more "spread out" than the original G. Like rescaling by the magnitude to the derivative, this operator can be viewed as a rescaling.

Remark 2 Using the inner product $\langle u, v\rangle_{H^1,A} = \langle Du, ADv\rangle_{L^2}$ for positive definite matrices A, a more general H^1 gradient can be defined. For example, a simple rescaling $\langle u, v\rangle_{H^1,\alpha,\beta} = \alpha \langle u, v\rangle_{L^2} + \beta \langle \nabla u, \nabla v\rangle_{L^2}$ yields the following gradient: $\nabla_{H^1,\alpha,\beta} E = (\alpha I - \beta \Delta)^{-1}(\nabla_{L^2} E)$, for $\alpha, \beta > 0$. In our problem, it would be appropriate to choose $\alpha = 1$ and $\beta = \mu$, since that norm naturally appears in the energy, but for consistency between results, we set both to 1.

For further applications of Sobolev gradients to imaging problems, see [2, 13, 29, 32].

3 Analytical Remarks

In this section, we will analyze our approximation by showing that our model is consistent with the MS functional, via point-wise convergence, and discuss its relation to the other level set based segmentation models by looking at degenerate cases.

3.1 Consistency with the Mumford-Shah Functional

To derive our proposed energy, recall that we defined the subregions Ω_j $0 \le j \le 2$, where $\Omega \setminus \Gamma = \cup_j \Omega_j$, by the following characteristic functions: $\chi_1 = H(\phi)$, $\chi_2 = H(\psi)(1 - H(\phi))$, and $\chi_0 = (1 - H(\psi))(1 - H(\phi))$. Using these regions, the reconstructed function is defined by two auxiliary functions, u_1 and u_2, as follows: $u = u_1\chi_1 + u_2\chi_2 + \left(\frac{u_1+u_2}{2}\right)\chi_0$. Using these definitions, the L^2 norm in equation (1) becomes:

$$
\begin{aligned}
\int_\Omega |u - f|^2 dx &= \int_{\Omega_1} |u - f|^2 dx + \int_{\Omega_2} |u - f|^2 dx \int_{\Omega_0} |u - f|^2 dx \\
&= \int_{\Omega_1} |u_1 - f|^2 dx + \int_{\Omega_2} |u_2 - f|^2 dx + \int_{\Omega_0} \left|\frac{u_1 + u_2}{2} - f\right|^2 \chi_0 dx \\
&= \int_\Omega \left(|u_1 - f|^2 \chi_1 + |u_2 - f|^2 \chi_2 + \left|\frac{u_1 + u_2}{2} - f\right|^2 \chi_0 \right) dx
\end{aligned}
$$

and the H^1 semi-norm on $\Omega \setminus \Gamma$ in equation(1) becomes:

$$
\begin{aligned}
\int_{\Omega\setminus\Gamma} |\nabla u|^2 dx &= \int_{\Omega_1} |\nabla u|^2 dx + \int_{\Omega_2} |\nabla u|^2 dx + \int_{\Omega_0} |\nabla u|^2 dx \\
&= \int_{\Omega_1} |\nabla u_1|^2 dx + \int_{\Omega_2} |\nabla u_2|^2 dx + \int_{\Omega_0} \left|\nabla \left(\frac{u_1 + u_2}{2}\right)\right|^2 dx \\
&= \int_{\Omega} |\nabla u_1|^2 \chi_1 dx + \int_{\Omega} |\nabla u_2|^2 \chi_2 dx + \int_{\Omega} \left|\nabla \left(\frac{u_1 + u_2}{2}\right)\right|^2 \chi_0 dx \\
&= \int_\Omega \left(|\nabla u_1|^2 (\chi_1 + \frac{\chi_0}{4}) + \mu |\nabla u_2|^2 (\chi_2 + \frac{\chi_0}{4}) + \frac{\mu}{2} \nabla u_1 \cdot \nabla u_2 \chi_0 \right) dx
\end{aligned}
$$

ignoring measure zero terms. Lastly, the length term in equation(1) becomes:

$$
\text{Length}(\Gamma) = \int_\Gamma ds = \int_{\phi=0} H(\psi) ds = \int_\Omega |\nabla H(\phi)| H(\psi) = \int_\Omega \chi_3 \, |\nabla \chi_1|
$$

where the equation above is in the sense of measures and $H' = \delta$, the Dirac delta function. All together, these three terms make up our proposed energy. In order to formally take the Euler-Lagrange equations, each Heaviside function is replaced with a smooth approximation, also yielding a continuous approximation to the delta function.

There is much freedom in the choice of approximations. In general, given any function $\delta_1 \in C^0$ such that $\int_{\mathbb{R}} \delta_1(x) dx = 1$, one can construct an approximation to the Dirac delta function by setting $\delta_\epsilon(x) := \frac{1}{\epsilon}\delta_1\left(\frac{x}{\epsilon}\right)$ and an approximation to the Heaviside function by setting $H_\epsilon(x) := \int \delta_\epsilon(x) dx$. This yields the following properties:

1. $H_\epsilon(x) \to H(x)$ point-wise everywhere except at $x = 0$

2. $\delta_\epsilon = H'_\epsilon$
3. $H_\epsilon \in C^1$

These conditions are easily satisfied by our particular choice of approximations: $H_\epsilon(x) = \frac{1}{2} + \frac{1}{\pi} arctan\left(\frac{x}{\epsilon}\right)$ and $\delta_\epsilon(x) = \frac{1}{\pi}\frac{\epsilon}{\epsilon^2+x^2}$.

As ϵ goes to zero, the approximations to the L^2 error term and H^1 regularity term converge to their un-regularized forms (by Lebesgue Dominated Convergence). For the length term, the following theorem is provided, see also [6].

Theorem 2 *Let $L_\epsilon(\phi,\psi) = \int_\Omega |\nabla H_\epsilon(\phi)| H_\epsilon(\psi)$ with H_ϵ satisfying the properties above and let ϕ and ψ be Lipschitz continuous; then*

$$\lim_{\epsilon\to 0} L_\epsilon(\phi,\psi) = \int_{\{\phi=0\}} H(\psi)ds = Length(\Gamma)$$

where $\Gamma := \{x \in \Omega \Big| \ \phi(x) = 0, \psi(x) > 0\}$.

Proof Using the co-area formula (see [10]) and the fact that H_ϵ is smooth, the regularized length becomes:

$$\begin{aligned} L_\epsilon(\phi,\psi) &= \int_{\mathbb{R}} \left(\int_{\phi=\rho} \delta_\epsilon(\phi) H_\epsilon(\psi) ds \right) d\rho \\ &= \int_{\mathbb{R}} \delta_\epsilon(\rho) \left(\int_{\phi=\rho} H_\epsilon(\psi) ds \right) d\rho. \end{aligned}$$

Define $S_\epsilon(\rho) := \int_{\phi=\rho} H_\epsilon(\psi)ds$. By the scalability property of the delta function,

$$\begin{aligned} L_\epsilon(\phi,\psi) &= \int_{\mathbb{R}} \delta_\epsilon(\rho) S_\epsilon(\rho) d\rho \\ &= \int_{\mathbb{R}} \frac{1}{\epsilon}\delta_1\left(\frac{\rho}{\epsilon}\right) S_\epsilon(\rho) d\rho \end{aligned}$$

By the change of variable $p = \frac{\rho}{\epsilon}$, we obtain

$$\begin{aligned} \lim_{\epsilon\to 0} L_\epsilon(\phi,\psi) &= \lim_{\epsilon\to 0} \int_{\mathbb{R}} \delta_1(p) S_\epsilon(\epsilon p) dp \\ &= S_0(0) \int_{\mathbb{R}} \delta_1(p) dp = S_0(0) \\ &= \int_{\phi=0} H(\psi) ds = \text{Length}(\Gamma), \end{aligned}$$

It is clear that $S_0(0) = \int_{\phi=0} H(\psi)ds$, since

$$\begin{aligned} S_\epsilon(\epsilon p) - S_0(0) &= \int_{\phi=\epsilon p} H_\epsilon(\psi) ds - \int_{\phi=0} H(\psi) ds \\ &= \left(\int_{\phi=\epsilon p} H_\epsilon(\psi) ds - \int_{\phi=\epsilon p} H(\psi) ds \right) - \left(\int_{\phi=\epsilon p} H(\psi) ds - \int_{\phi=0} H(\psi) ds \right) \\ &= \left(\int_{\phi=\epsilon p} \left(H_\epsilon(\psi) - H(\psi)\right) ds \right) - \left(\int_{\phi=\epsilon p} H(\psi) ds - \int_{\phi=0} H(\psi) ds \right) \end{aligned}$$

Since $H_\epsilon(x) \to H(x)$ in $\mathbb{R} \setminus \{0\}$ and since the length of the level sets are finite, the first term goes to zero, while the second term goes to zero by continuity of the integral.

3.2 Relation to Other Models

In practice, the curve Γ can change its topology freely. Even if it is initialized with free endpoints, it may become an endpoint free curve, or vice versa. The standard splitting and merging behavior now includes breaking (or cracking) where, during its evolution, the curve can crack itself to develop endpoints. With this addition, our model can be viewed as a natural extension to other level set based methods for segmentation. Here we briefly examine the degeneration of the energy (and thus the curve evolution) into the classical models.

Firstly, the model can completely degenerate to the endpoint free structure when the indicator level set function has fixed sign, *i.e.* $\psi > 0$. The characteristic functions become:

$$\begin{aligned}
\chi_1 &= H(\phi) \\
\chi_2 &= H(\psi)(1 - H(\phi)) = 1 - H(\phi) \\
\chi_3 &= H(\psi) = 1 \\
\chi_0 &= (1 - H(\psi))(1 - H(\phi)) = 0
\end{aligned}$$

and the reconstruction function takes the form:

$$\begin{aligned}
u &= u_1\chi_1 + u_2\chi_2 + \left(\frac{u_1 + u_2}{2}\right)\chi_0 \\
&= u_1 H(\phi) + u_2(1 - H(\phi))
\end{aligned}$$

Thus the function is smooth in each of the two regions defined by the sign of ϕ. The energy becomes:

$$\begin{aligned}
E(u_1, u_2, \phi, -) = \mu \int_\Omega |\nabla u_1|^2 H(\phi) + |\nabla u_2|^2 (1 - H(\phi))dx + \lambda \int_\Omega |\nabla H(\phi)| \\
+ \int_\Omega \left(|u_1 - f|^2 H(\phi) + |u_2 - f|^2 (1 - H(\phi))\right) dx
\end{aligned}$$

which is the two-phase piece-wise smooth Chan-Vese model. Furthermore, if the regularization parameter is set to a large value, $\mu >> 1$, or if u is restricted to the set of piece-wise constant solutions, and where $u_1 = c_1$ and $u_2 = c_2$, where $c_1, c_2 \in \mathbb{R}$, then the reconstruction function becomes $u = c_1 H(\phi) + c_2(1 - H(\phi))$ and the energy becomes:

$$E(c_1, c_2, \phi, -) = \lambda \int_\Omega |\nabla H(\phi)| + \int_\Omega \left(|c_1 - f|^2 H(\phi) + |c_2 - f|^2 (1 - H(\phi))\right) dx$$

which recovers the two-phase piecewise constant Chan-Vese model.

4 Numerical Method

Since the model is non-convex and highly non-linear, an alternating minimization is used, where the energy is minimized with respect to each variable separately. During each minimization, three steps are done: calculate the Euler-Lagrange equation, find the Sobolev gradient, and step forward in time.

To calculate the Euler-Lagrange equations, the PDEs are discretized using forward differences for the gradient and backwards differences for the divergence, in order to retain their adjoint relationship. The magnitudes of the gradient are replaced with a regularized version to avoid dividing by zero. With respect to the time discretization, the Euler-Lagrange equation is completely explicit and the inversion of the preconditioning operator (Sobolev gradient) is done using a semi-implicit method. Specifically, let $G = -\nabla_{L^2} E$ be the Euler-Lagrange equation and v equals the Sobolev gradient. Then we have the relationship from before: $v - \Delta v = G$, which we solve using a Gauss-Seidel sweep of the following discretization:

$$v_{i,j}^{n+1} - \left(v_{i+1,j}^{n} - 2v_{i,j}^{n+1} + v_{i-1,j}^{n}\right) - \left(v_{i,j+1}^{n} - 2v_{i,j}^{n+1} + v_{i,j-1}^{n}\right) = G_{i,j}$$

In practice, a few iterations are sufficient. Alternatively, v can be found using the Fourier transform: $v = \mathcal{F}^{-1}\left(\frac{\mathcal{F}(G)}{1+|\xi|^2}\right)$. Once v is found, a forward Euler step is used to update the variable (recall that the time derivative of the variable is equal to the Sobolev gradient of the energy).

Next, with respect to the boundary conditions for the reconstructed image, if the auxiliary functions u_1 and u_2 are initialized to have Neumann boundary conditions at $t = 0$, then in semi-discrete terms the future boundary conditions are:

$$\begin{aligned} \chi_1 \frac{\partial}{\partial N} u_1^{n+1} + \frac{\chi_0}{4} \frac{\partial}{\partial N}(u_1^{n+1} + u_2^{n}) \quad &= 0 \\ \chi_2 \frac{\partial}{\partial N} \nabla u_2^{n+1} + \frac{\chi_0}{4} \frac{\partial}{\partial N}(u_1^{n+1} + u_2^{n+1}) &= 0 \end{aligned}$$

Since the characteristic functions are assumed to be nonzero everywhere (based on our choice of approximations):

$$\begin{aligned} \frac{\partial}{\partial N} u_1^{n+1} &= -\frac{\chi_0}{4\chi_1 + \chi_0} \frac{\partial}{\partial N} u_2^{n} \\ \frac{\partial}{\partial N} u_2^{n+1} &= -\frac{\chi_2}{4\chi_2 + \chi_0} \frac{\partial}{\partial N} u_1^{n+1} \end{aligned}$$

Since $\frac{\partial}{\partial N} u_1^0 = \frac{\partial}{\partial N} u_2^0 = 0$, they stay that way for all $n > 0$.

This process is iterated until convergence with respect to one variable is achieved, and then each of these alternating steps are repeated until total convergence. In terms of the level set functions, ϕ and ψ, only partial convergence is needed.

Lastly, once the updates for u_1 and u_2 are found in order to calculate the various differences across the curve Γ for the level set equations, each function needs to be extended. In general, any C^1 extension is approriate; in particular, we solve $\Delta u_1 = 0$ in region 2 and $\Delta u_2 = 0$ in region 1 with prescribed boundary conditions (Dirchelet), and the extensions are labelled Eu_1 and Eu_2. Altogether the algorithm is given below.

Algorithm

Initialize $u_1^0, u_2^0, \phi^0, \psi^0$

while Not Converged **do**

Substep 1: Compute $G_{u_1}(u_1^n, u_2^n, \phi^n, \psi^n)$, Solve for $v_{u_1}^n$, Iterate Forward to u_1^{n+1}

Substep 2: Compute $G_{u_2}(u_1^{n+1}, u_2^n, \phi^n, \psi^n)$, Solve for $v_{u_2}^n$, Iterate Forward to u_2^{n+1}

Substep 3: Extend u_1^{n+1} and u_2^{n+1} to Eu_1^{n+1} and Eu_2^{n+1}

Substep 4: Compute $G_{\phi}(Eu_1^{n+1}, Eu_2^{n+1}, \phi^n, \psi^n)$, Solve for v_{ϕ}^n, Iterate Forward to ϕ^{n+1}

Substep 5: Compute $G_{\psi}(Eu_1^{n+1}, Eu_2^{n+1}, \phi^{n+1}, \psi^n)$, Solve for v_{ψ}^n, Iterate Forward to ψ^{n+1}

end while

The convergence is typically measured by the difference in energy between the two iterations. Compared to the general level set based segmentation methods, this algorithm is more sensitive to initialization. In the standard methods, if the curve were to be initialized as a large circle that encloses all the objects, then it would shrink inward until it captured all the edges. In our case, if the curve was initialized as a large arc, it may shrink along the curve more quickly than inward (shrinking along the tangents rather than the normal vectors). In general, this can be controlled by the number of iterations in Substeps 4 and 5 or by initializing the curve to intersect the desired edges. This can be done in practice by over-segmenting the image using classical edge-detectors and then using the result to provide regions of interest for initializations.

4.1 Further Remarks

In terms of the forward Euler step in our method, starting from the same data, the Sobolev gradient decreases the energy more than the L^2 descent.

Theorem 3 *Let ΔE_S and ΔE_{L^2} be the discrete changes in energy using Sobolev and L^2 gradient descent, receptively. Starting at the same value, if Δt_S and Δt_{L^2} are the time steps for the discretization of the Sobolev and L^2 gradient descent algorithm, repectively, then $\Delta E_S = \Delta E_{L^2} \frac{\Delta t_S}{\Delta t_{L^2}}$.*

Proof Let $v = \nabla_{H^1} E(\phi)$ and $G := \nabla_{L^2} E(\phi)$ then we have $(I - \Delta)v = G$ in a weak sense with Neumann conditions. This equation is the weak formulation of the problem: for all $h \in H^1(\Omega)$

$$\int_\Omega [vh + \nabla v \cdot \nabla h]\, dx = \int_\Omega Gh\ dx$$

which is equivalent to

$$\langle v, h\rangle_{H^1(\Omega)} = G(h) \tag{7}$$

where $G(h)$ is the linear form from the right hand side of the weak equation. Assuming that $G \in H^{-1}(\Omega)$, by the Riesz Representation theorem, there exists a unique $g \in H^1(\Omega)$ such that $G(h) = \langle g, h\rangle_{H^1(\Omega)}$ for all $h \in H^1(\Omega)$ (or equivalently by the Lax-Milgram theorem) and $||G||_{H^{-1}} = ||g||_{H^1}$. Combing this with the equation above yields $\langle v - G, h\rangle_{H^1} = 0$. Therefore we can see that $v = g$ *a.e.* and $||G||_{H^{-1}} = ||v||_{H^1}$

If we look at the ratio of changes in energy at a given iteration with Euler time steps then we have

$$\frac{\Delta E_S}{\Delta E_{L^2}} = \frac{\Delta t_S ||s||^2_{H^1}}{\Delta t_{L^2} ||r||^2_{L^2}} = \frac{\Delta t_S}{\Delta t_{L^2}}$$

Note that since we assumed $r \in L^2$, we have that the H^{-1} norm is just the L^2 norm of r.

In general, the preconditioned PDEs are more stable, which lets $\Delta t_S \geq \Delta t_{L^2}$, so that we will almost always get $\Delta E_S \geq \Delta E_{L^2}$. We see that not only is the Sobolev descent method better posed theoretically, it is also preferred numerically.

5 Experimental Results

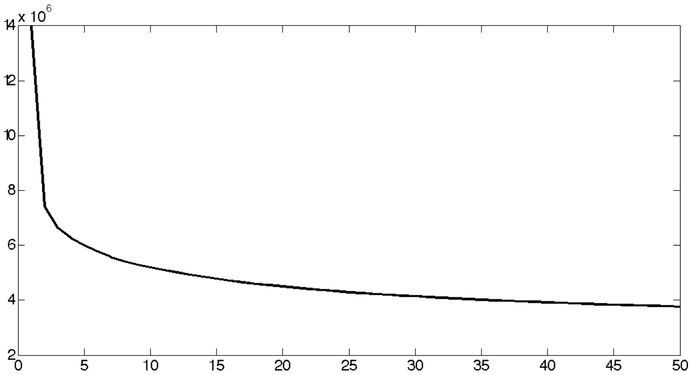

Fig. 2 Plot of Energy verse Iteration using Sobolev Gradient descent

We use time steps $\Delta t \in [.01, .1]$, space steps $\Delta x = 1$, and $\epsilon = \Delta x$. Without the Sobolev gradient, Δt must be very small to guarantee stability, which in many cases incurs other numerical issues. The number of iterations in each minimization step for u_1 and u_2 is set to a maximum of about 150 (although they converges before reaching the maximal amount of iterations), while the level set minimization steps are set to a maximum of about 2-5 iterations. The algorithm converges between several seconds and a few minutes depending on the size of the image. In these examples, no re-initialization is used for the level set function. In Figure 2, the energy for the edge case is plotted against the number of iteration and is strictly decreasing.

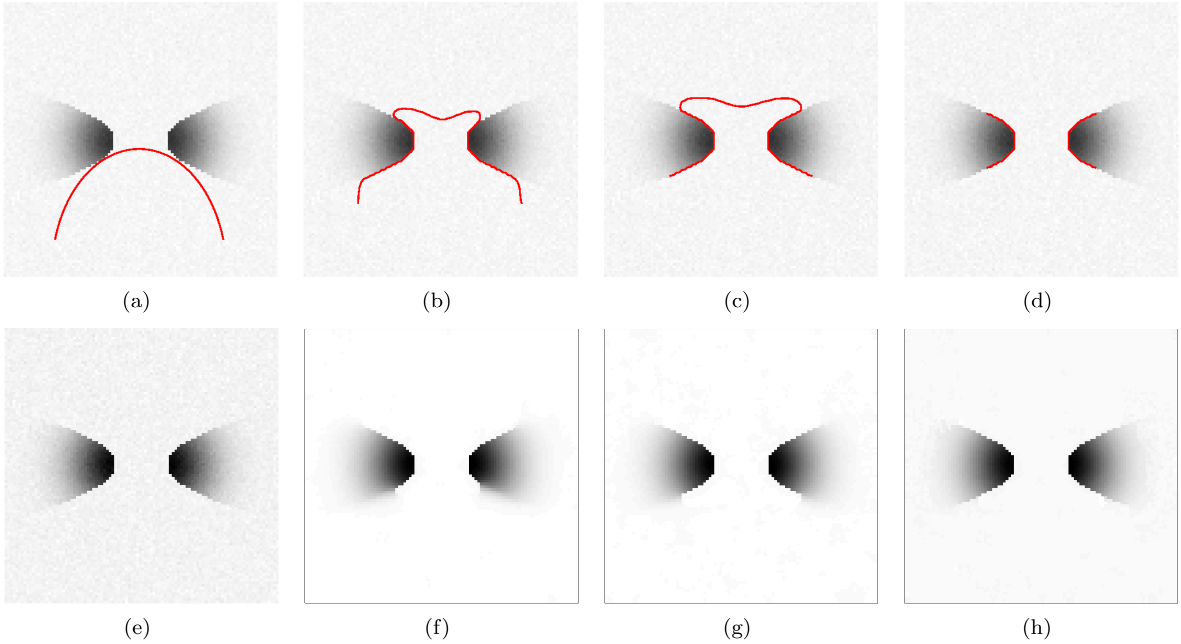

Fig. 3 Segmentation and Restoration of a Synthetic Image with Two Free Edge Sets: the curve evolution (a-d) and the restoration (e-h) with $\mu = 4$ and $\lambda = .02 * 255^2$.

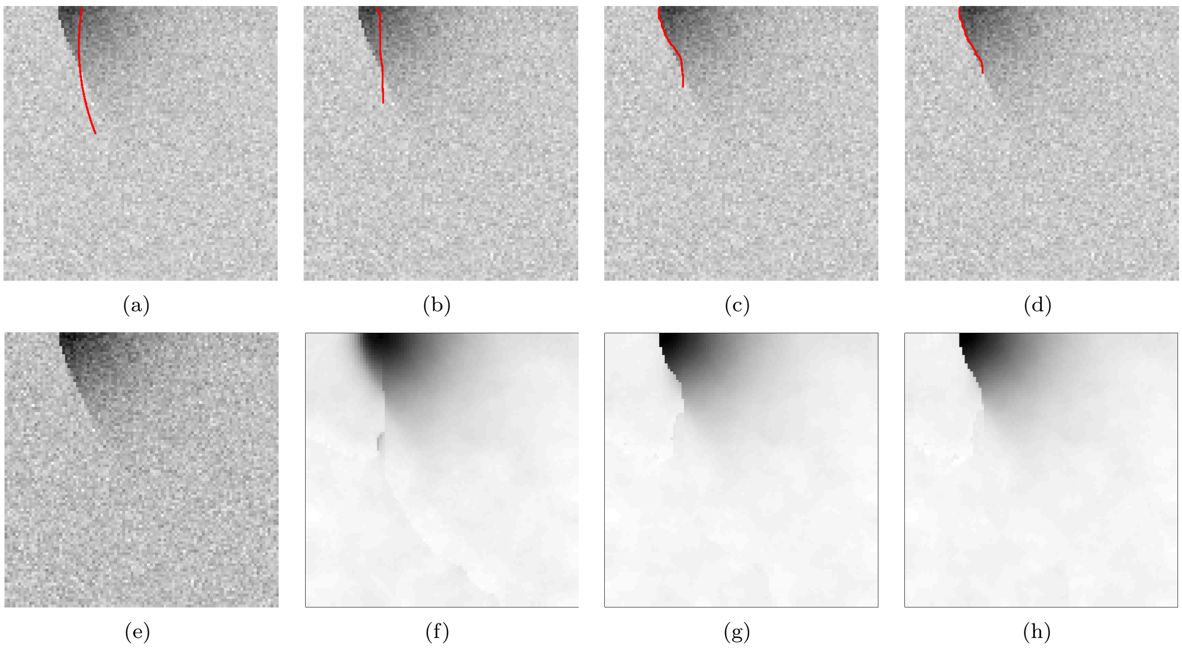

Fig. 4 Segmentation and Restoration of a Synthetic Image with a Half Edge: $\mu = 17$ and $\lambda = .01 * 255^2$.

In Figure 3, the method is applied to a noisy synthetic image with an edge set comprised of two free curves. The initial curve is made up of one segment, which first locates the edges and then separates into two segments (taking only a few iterations to break topology). In Figure 4, the method is applied to a very noisy synthetic image with an edge that has one endpoint which terminates at the boundary of the image and one endpoint that is free. The curve is initialized near the edge and the algorithm converges in seconds. In Figure 5, the method is applied to a noisy synthetic image comprised of one segment with endpoints and one without endpoints. The curve is initialized as two circles, but one breaks its topology in order to capture the free endpoint structure. From these examples, the results depict the robustness of the algorithm to the varying edge structures.

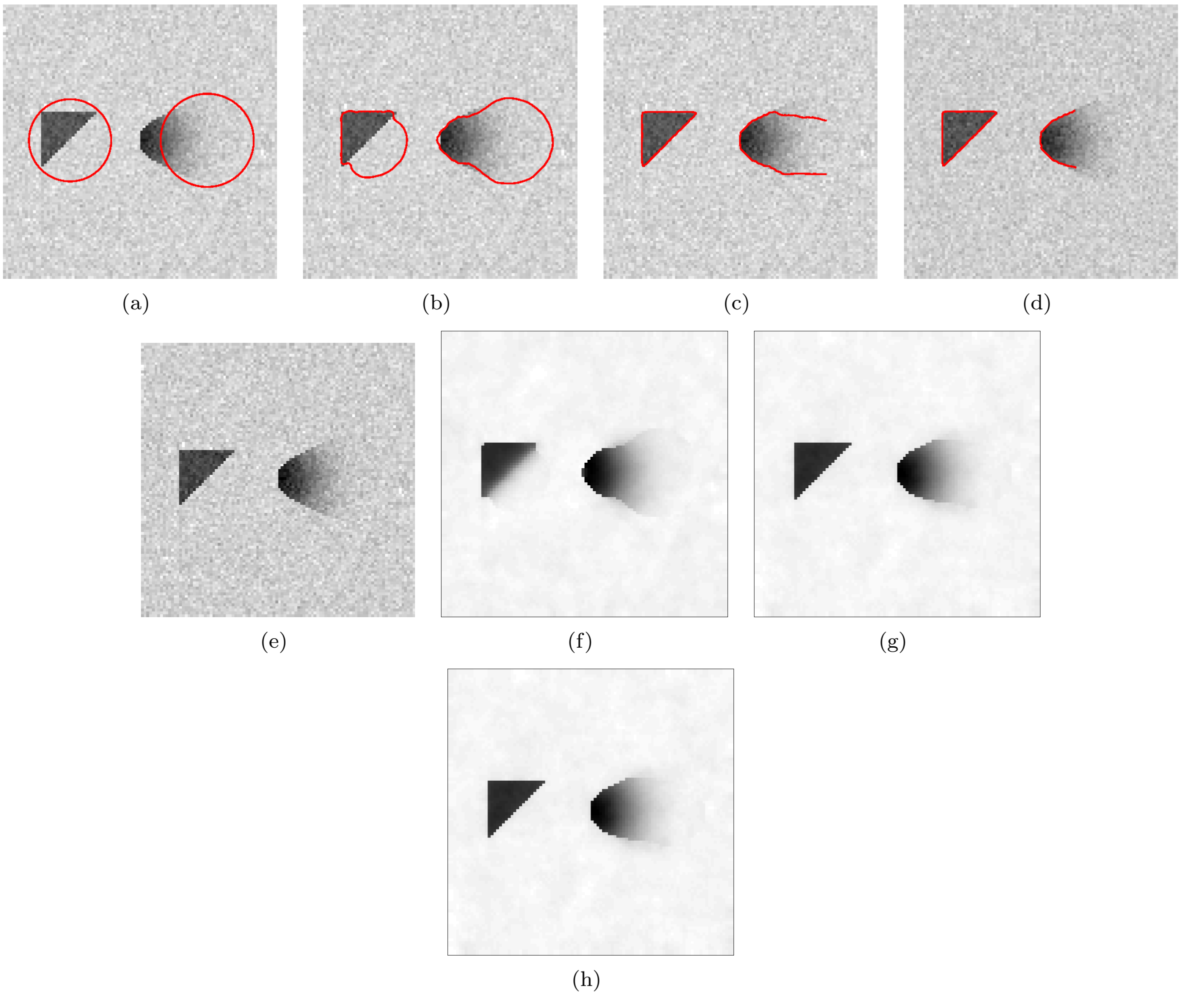

Fig. 5 Segmentation and Restoration of a Synthetic Image with Different Topologies: $\mu = 5$ and $\lambda = .05 * 255^2$.

The method is also applied to two real images: one of a comet and the other of a plasma. In Figure 6, the curve locates the front of the comet, and the restored image sharpens the contrast between the comet and the background and removes noise from the comet, while preserving large stars (point structures) in the background. The final segmentation is compared to other techniques in Figure 7. The Chan-Vese method locates the correct front, but over segments the comet, since it must be a loop. The Canny edge detector over-segments the white interior region of the comet, missing the faint boundary which defines the comet front. Similarly, the Ambrosio-Tortorelli method mainly locates the white region, where the gradient is sharpest.

Lastly, we test our algorithm on a real plasma image. In Figure 8, the curve locates the plasma front and the restored image sharpens the contrast between the plasma front and the background, while removing the small amount of noise present in the image. This particular segmentation is made difficult by the light region in the top left quadrant near the plasma front. Region based methods would try to group the lighter intensities together, avoiding the actual edge. The final segmentation is compared to other techniques in Figure 9. The Chan-Vese method does not properly locate the edge, since it does not enclose a region. The Canny edge detector does not locate the correct edge – locating places of high gradient inside of the plasma. Similarly, the Ambrosio-Tortorelli method does locate the front correctly but also includes excess edges, which cannot be removed by thresholding.

6 Acknowledgments

This research was made possible with Government support under and awarded by the Department of Defense (DoD) through the National Defense Science and Engineering Graduate Fellowship (NDSEG)

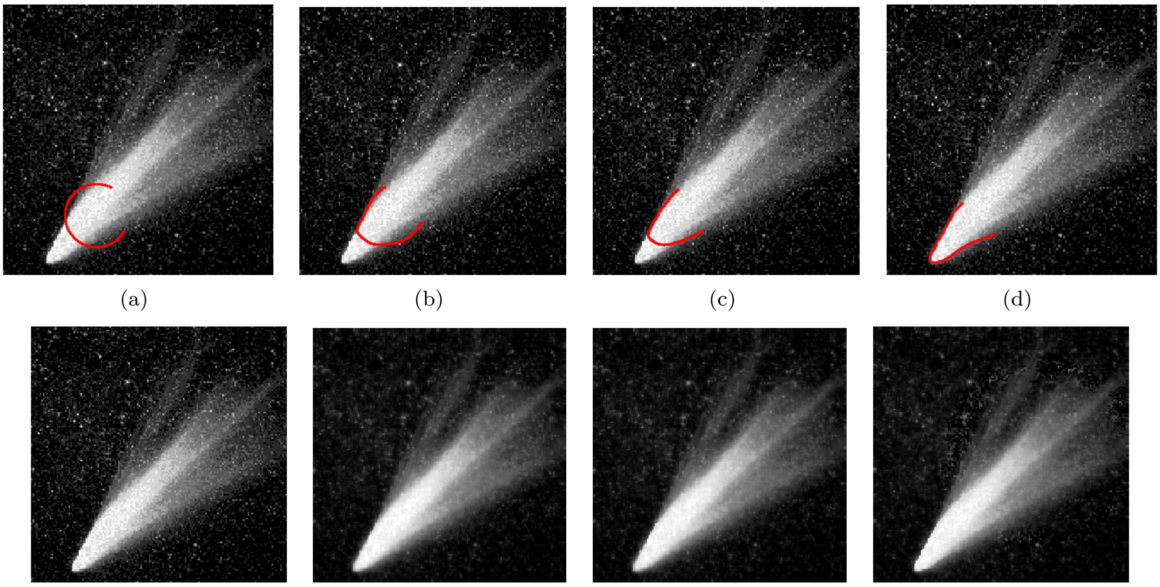

(a) (b) (c) (d)

(e) (f) (g) (h)

Fig. 6 Segmentation and Restoration of a Comet with Noise: $\mu = .5$ and $\lambda = .01 * 255^2$

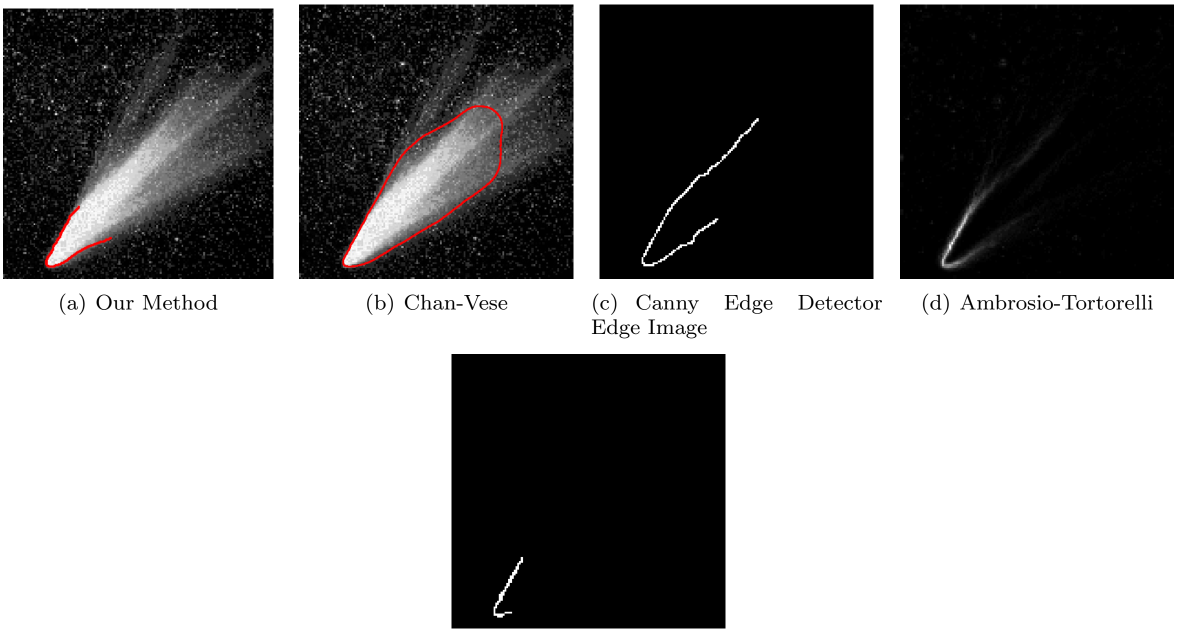

(a) Our Method

(b) Chan-Vese

(c) Canny Edge Detector Edge Image

(d) Ambrosio-Tortorelli

(e) Ambrosio-Tortorelli Edge Image after thresholding

Fig. 7 Comparison

Program and in part by the National Science Foundation Grant DMS 0714945 and CCF/ITR Expeditions Grant 0926127.

7 Conclusion

We have proposed an extension to the level set based image segmentation method that detects free endpoint structures. By generalizing the curve representation used in the Active Contour model to also include free endpoint structures, we are able to segment a larger class of images with a variety of edge structures. This

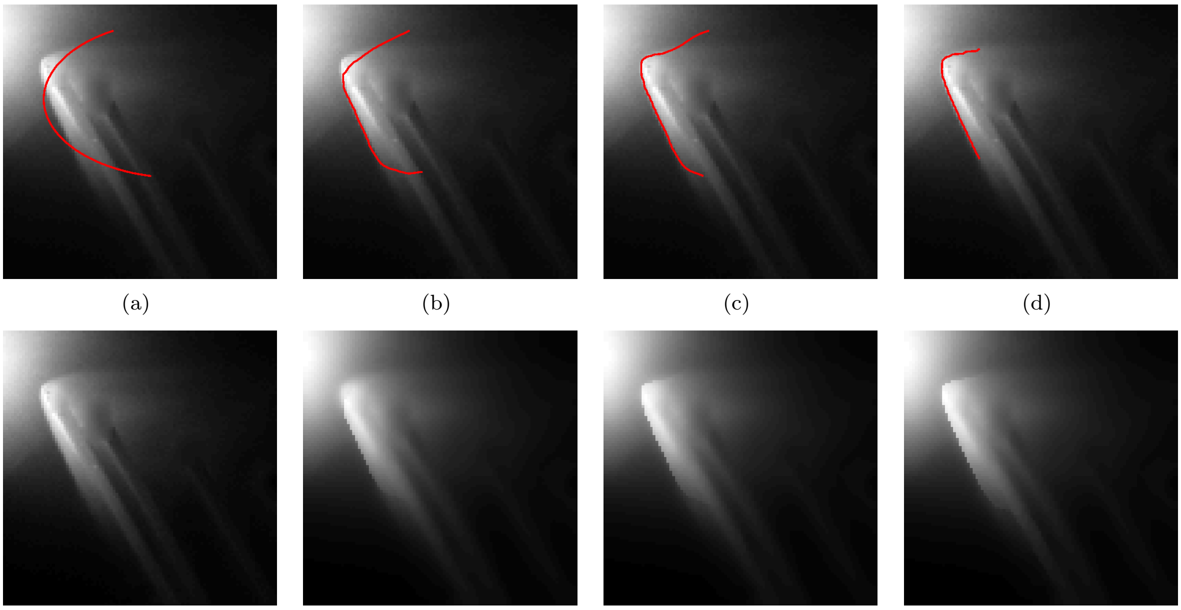

(a) (b) (c) (d)

(e) (f) (g) (h)

Fig. 8 Segmentation and Restoration of a Plasma at UCLA [25]: $\mu = 25$ and $\lambda = .8 * 255^2$

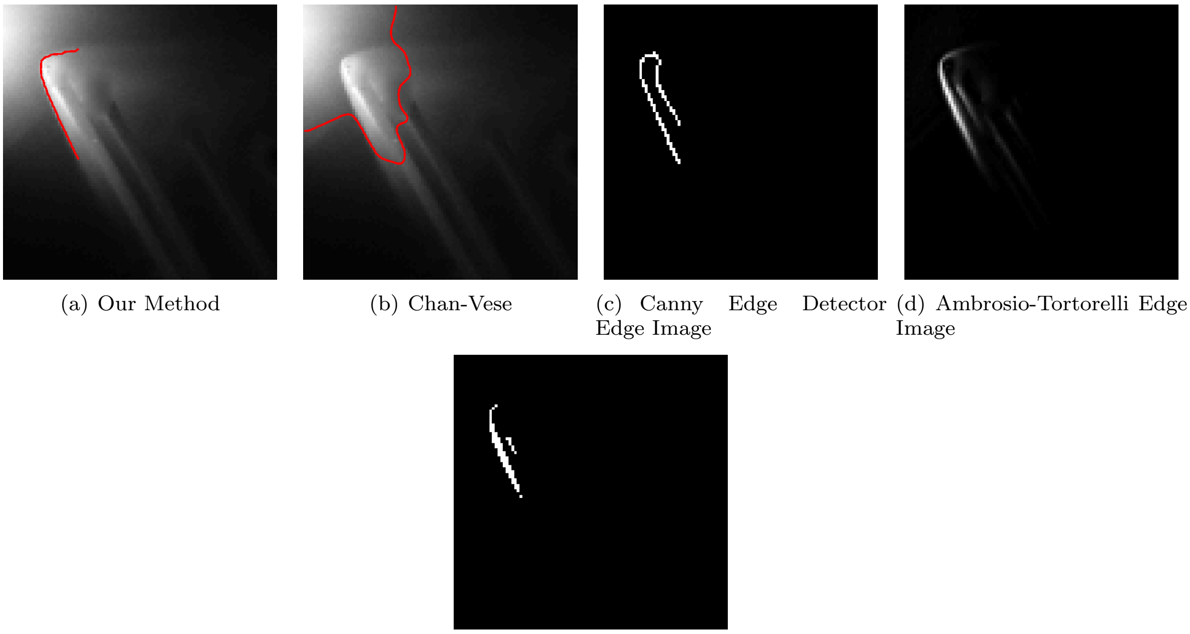

(a) Our Method (b) Chan-Vese (c) Canny Edge Detector Edge Image (d) Ambrosio-Tortorelli Edge Image

(e) Ambrosio-Tortorelli Edge Image after thresholding

Fig. 9 Comparison

proposed method is able to change its topology by splitting, merging, and now breaking curves without endpoints into free curves and vice versa. The results were tested on both synthetic and real images and in the examples presented in this work, were more successful in locating the correct edge set as compared to standard methods.

References

1. L. Ambrosio and V. M. Tortorelli. Approximation of functional depending on jumps by elliptic functional via t-convergence. *Communications on Pure and Applied Mathematics*, 43(8):999–1036, December 1990.
2. L. Bar and G. Sapiro. Generalized Newton-Type methods for energy formulations in image processing. *SIAM Journal on Imaging Sciences*, 2(2):508, 2009.
3. R. Caselles, V.and Kimmel and G. Sapiro. Geodesic active contours. *International Journal of Computer Vision*, 22(1):61–79, 1997.
4. T. F. Chan, B. Y. Sandberg, and L. A. Vese. Active contours without edges for Vector-Valued images. *Journal of Visual Communication and Image Representation*, 11(2):130–141, June 2000.
5. T.F. Chan and L.A. Vese. Active contours without edges. *IEEE Transactions on Image Processing*, 10(2):266–277, February 2001.
6. G. Chung and L. A. Vese. Image segmentation using a multilayer level-set approach. *Computing and Visualization in Science*, 12(6):267–285, April 2008.
7. L. D. Cohen and R. Kimmel. Global minimum for active contour models: A minimal path approach. *International Journal of Computer Vision*, 24(1):57–78, 1997.
8. M.G. Crandall, L.C. Evans, and R.F. Gariepy. Optimal lipschitz extensions and the infinity laplacian. *Calculus of Variations and Partial Differential Equations*, 13(2):123–139, 2001.
9. G. Dal Maso, J. M. Morel, and S. Solimini. A variational method in image segmentation: Existence and approximation results. *Acta Mathematica*, 168(1):89–151, 1992.
10. L. C. Evans and R. F. Gariepy. *Measure Theory and Fine Properties of Functions*. CRC Press, 1992.
11. L. C. Evans and Y. Yu. Various properties of solutions of the Infinity-Laplacian equation. *Communications in Partial Differential Equations*, 30(9):1401–1428, September 2005.
12. E. Giorgi, M. Carriero, and A. Leaci. Existence theorem for a minimum problem with free discontinuity set. *Archive for Rational Mechanics and Analysis*, 108(4):195–218, 1989.
13. M. Jung, G. Chung, G. Sundaramoorthi, L. A. Vese, and A. L. Yuille. Sobolev gradients and joint variational image segmentation, denoising, and deblurring. *Proceedings of SPIE*, 7246(1):72460I–72460I–13, February 2009.
14. M. Kass, A. Witkin, and D. Terzopoulos. Snakes: Active contour models. *International Journal of Computer Vision*, 1(4):321–331, 1988.
15. R. Kimmel and A. M. Bruckstein. Regularized laplacian zero crossings as optimal edge integrators. *International Journal of Computer Vision*, 53:225–243, 2001.
16. C. Lacoste, X. Descombes, and J. Zerubia. Unsupervised line network extraction in remote sensing using a polyline process. *Pattern Recognition*, 43(4):1631–1641, April 2010.
17. C. J. Larsen, C. L. Richardson, and M. Sarkis. A level set method for the mumford -Shah functional and fracture. *Preprint serie A,Instituto Nacional de Matemática Pura e Aplicada, Brazilian Ministry for Science and Technology*, (2008).
18. W. H. Liao, L. Vese, S. C. Huang, M. Bergsneider, and S. Osher. Computational anatomy and implicit object representation: A level set approach. In James Gee, J. Maintz, and Michael Vannier, editors, *Biomedical Image Registration*, volume 2717 of *Lecture Notes in Computer Science*, pages 40–49. Springer Berlin / Heidelberg, 2003.
19. G. Lu and P. Wang. Inhomogeneous infinity laplace equation. *Advances in Mathematics*, 217(4):1838–1868, March 2008.
20. J. Melonakos, E. Pichon, S. Angenent, and A. Tannenbaum. Finsler active contours. *Pattern Analysis and Machine Intelligence, IEEE Transactions on*, 30(3):412 –423, March 2008.
21. J. M. Morel and S. Solimini. Segmentation of images by variational methods: a constructive approach. *Revista Matematica de la Universidad Complutense de Madrid*, 1:169–182, 1988.
22. J. M. Morel and S. Solimini. Segmentation d'images par méthode variationnelle: une preuve constructive d'existence. *Comptes rendus de l'Académie des sciences. Série 1, Mathématique*, 308(15):465–470, 1989.
23. D. Mumford and J. Shah. Optimal approximations by piecewise smooth functions and associated variational problems. *Communications on Pure and Applied Mathematics*, 42(5):577–685, July 1989.
24. J. W. Neuberger. *Sobolev Gradients and Differential Equations*. Springer, November 2009.
25. C. Niemann, A.S. Bondarenko, C.G. Constantin, E.T. Everson, K.A. Flippo, S.A. Gaillard, R.P. Johnson, S.A. Letzring, D.S. Montgomery, L.A. Morton, D.B. Schaeffer, T. Shimada, and D. Winske. Collisionless shocks in a large magnetized laser-plasma plume. *Plasma Science, IEEE Transactions on*, 39(11):2406 –2407, nov. 2011.
26. A. M. Oberman. A convergent difference scheme for the infinity laplacian: Construction of absolutely minimizing lipschitz extensions. *Mathematics of Computation*, 74(251):1217–1230., September 2004.
27. S. Osher and J. A Sethian. Fronts propagating with curvature-dependent speed: Algorithms based on Hamilton-Jacobi formulations. *Journal of Computational Physics*, 79(1):12–49, November 1988.
28. R J. Renka. A simple explanation of the sobolev gradient method, 2006.
29. W. B. Richardson. Sobolev gradient preconditioning for image-processing PDEs. *Communications in Numerical Methods in Engineering*, 24(6):493–504, December 2006.
30. J. Shen. Piecewise $h^{-1} - h^0 - h^1$ images and the mumford-shah-sobolev model for segmented image decomposition. *APPL. MATH. RES. EXP*, 4:2005, 2005.
31. P. Smereka. Spiral crystal growth. *Physica D: Nonlinear Phenomena*, 138(3–4):282–301, April 2000.
32. G. Sundaramoorthi, A. Yezzi, and A. C. Mennucci. Sobolev active contours. *International Journal of Computer Vision*, 73(3):345–366, January 2007.
33. A. Tsai, Jr. Yezzi, A., and A.S. Willsky. Curve evolution implementation of the Mumford-Shah functional for image segmentation, denoising, interpolation, and magnification. *Image Processing, IEEE Transactions on*, 10(8):1169 –1186, August 2001.
34. L. A. Vese and T. F. Chan. A multiphase level set framework for image segmentation using the mumford and shah model. *International Journal of Computer Vision*, 50(3):271–293, 2002.